AIAA JOURNAL
Vol. 40, No. 5, May 2002

Numerical Modeling of Axisymmetric and Three-Dimensional Flows in Microelectromechanical Systems Nozzles

Alina A. Alexeenko* and Deborah A. Levin†
Pennsylvania State University, University Park, Pennsylvania 16802
Sergey F. Gimelshein‡
George Washington University, Washington, D.C. 20052
Robert J. Collins§
University of Minnesota, Minneapolis, Minnesota 55455
and
Brian D. Reed¶
NASA John H. Glenn Research Center at Lewis Field, Cleveland, Ohio 44125

A numerical study of three-dimensional effects on the performance of a micronozzle fabricated from flat silicon wafers is performed by use of both continuum and kinetic approaches. The nozzle operates in a low-Reynolds-number regime, and viscous effects dominate the gas expansion. Thrust losses occur because the shear on the wall is greater in a flat nozzle configuration than in an axisymmetric conical nozzle. Therefore, the prediction of the micronozzle performance based on axisymmetric or two-dimensional modeling can lead to significant design errors. Comparison of simulation with recent data shows good agreement in terms of thrust predictions for cold-gas thrusters at Reynolds numbers of approximately 2×10^2.

I. Introduction

THE recent advances in microelectromechanical systems (MEMS) have led to the construction of various types of micrometer-scaled mechanical devices. Bulk micromachining of silicon and other materials has been used to produce pumps, small motors, channels, mechanical sensors, and other devices.[1] MEMS technology has also been considered for the production of micrometer-sized rocket motors; however, several questions must be addressed before their utility can be assessed. One of the most important issues is an estimate of the thrust performance at the small scale that is possible with this new technology.

The dramatic change in the linear dimension affects both the mechanics of the working fluid and geometric design of microdevices. From the fluid mechanics point of view, a model is needed to take into account microfluidic aspects.[2] A typical flow in a cold-gas micrometer-sized device has a low Reynolds number on the order of 10^2–10^3; therefore, viscous effects will be much more significant than in conventional large nozzles. Other consequences of the small linear scale for supersonic nozzle flows are rarefaction effects resulting in the possibility of velocity slip and temperature jump at the gas–solid surface interface. The surface area to volume ratio in microdevices is high, and the wall effects may dominate the fluid behavior inside the nozzle. Thus, accurate modeling of the fluid–surface interaction is required.

Conventional rocket nozzles are almost always of an axisymmetric shape and often have a contoured section to direct the exhaust gas along the axis. Because entirely different materials and manufacturing technology is used for MEMS, the geometric shape is different from that for large-scale nozzles. For the microfabrication of nozzle devices, the technique is well developed for etching a simple-shaped device from a silicon wafer. Experimental measurements by Bayt and Breuer[3] of mass flow and thrust levels in a flat contoured nozzle showed that for low Reynolds numbers, $Re < 5 \times 10^2$, nozzle performance is strongly affected by viscous losses and there is a considerable deviation from a two-dimensional Navier–Stokes solution because of the three-dimensional effects.

The main objectives of this present work are the numerical study of viscous effects in micronozzle flows and comparisons of different geometric configurations, axisymmetric conical and flat three dimensional, in terms of thrust performance and flowfields. A two-dimensional model of a micronozzle is also examined and compared with the full three-dimensional simulation.

Application of modern computational fluid dynamic techniques to model these flows can allow one to obtain detailed information on flow structure and peculiarities. There are two general approaches to treat a fluid in different flow regimes: continuum, when the scale of flow phenomena is large compared to the fluid microscopic structure, and kinetic, for a rarefied flow where phenomena at the molecular level become important. Because the flow regime varies from near continuum at the nozzle throat to rarefied at the nozzle exit, in micrometer-scale devices, accurate modeling is a challenging task for both approaches. Both kinetic and continuum numerical approaches are used in this study.

Several earlier papers presented computational results for axisymmetric micronozzle flows.[4–7] Most of them employed the direct simulation Monte Carlo (DSMC) method, the most widely used approach for modeling rarefied gas flows. The work by Chung et al.[5] was performed with the goal to make a comparison between numerical modeling and experimental data. In the paper by Ivanov et al.,[6] both DSMC and continuum methods were used to simulate the axisymmetric and two-dimensional flow in a nozzle at low Reynolds numbers.

The present paper is the first application of the DSMC method to the modeling of three-dimensional microthrusters. The solutions of the Navier–Stokes equations are also obtained to elucidate the area of applicability of the continuum approach. The paper also presents the first comparison of accurate experimental data with calculations for three-dimensional nozzles for $Re = 2 \times 10^2$. The earlier data of Bayt and Breuer[3] does not extend to such low Reynolds numbers.

The flow of molecular nitrogen in micronozzles is analyzed in terms of flowfields and performance characteristics. The outline of

Received 8 November 2000; revision received 13 September 2001; accepted for publication 17 October 2001.

*Graduate Research Assistant, Department of Aerospace Engineering. Student Member AIAA.
†Associate Professor, Department of Aerospace Engineering. Senior Member AIAA.
‡Senior Research Scientist, Department of Chemistry. Member AIAA.
§Professor Emeritus, Department of Electrical Engineering.
¶Research Engineer, On-Board Propulsion Branch. Member AIAA.

the paper is as follows. In Sec. II, the geometric setup and flow conditions are explained. Section III describes the numerical methods and computational requirements for the cases under consideration. Results of numerical modeling are presented in Sec. IV. A discussion of the flow features is also given, and the capabilities of numerical methods are compared. Finally, nozzle performance parameters are compared for different geometric configurations. Recent experimental thrust measurements of a flat micronozzle at $Re = 2 \times 10^2$ are presented and compared.[8]

II. Micronozzle Configurations and Flow Conditions

Two different micronozzle configurations are considered: axisymmetric and three dimensional. The axisymmetric conical nozzle has an expansion angle of 15 deg, a throat diameter $D_t = 300$ μm, and an exit-to-throat-area ratio of 100. A schematic of the three-dimensional (hereafter referred as flat) nozzle is shown in Fig. 1. The throat width is equal to the axisymmetric nozzle throat diameter D_t, and the height $h = 300$ μm. The expansion angle is 15 deg, and the area ratio is 10. The flat nozzle dimensions are derived from a recent experimental study.[9] The flat nozzle has the same cross section in the XY symmetry plane as the axisymmetric nozzle, as well as the same nozzle length of 5.038 mm. The details on nozzle geometry and computational domain in XY symmetry plane are given in Fig. 2.

For the two geometric nozzle configurations, the flow of molecular nitrogen was calculated at a stagnation pressure $p_c = 10$ kPa and stagnation temperature $T_c = 300$ K. Stagnation and critical conditions for a sonic flow at the throat are given in Table 1. The Knudsen number at the throat for both nozzles is 5×10^{-3}, and the corresponding Reynolds number based on the throat half-width is 2×10^2. The temperature at the nozzle wall is assumed to be constant and equal to the stagnation temperature at the chamber.

Table 1 Flow conditions (test gas, N_2)

Parameter	Value
Stagnation temperature T_c	300 K
Stagnation pressure p_c	10 kPa
Critical pressure p_t	5.2 kPa
Critical temperature T_t	250 K
Wall temperature T_w	300 K

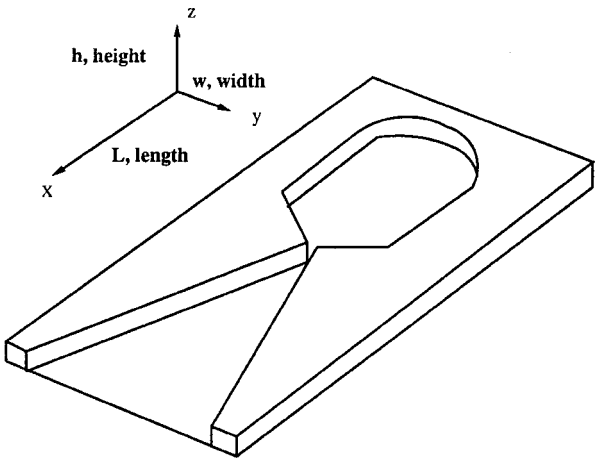

Fig. 1 Schematic of flat micronozzle.

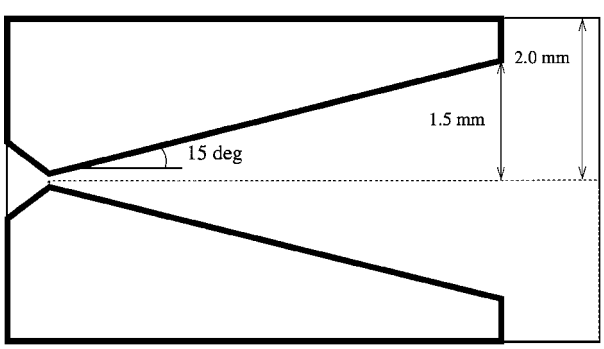

Fig. 2 Nozzle geometry and computational domain in XY plane.

III. Numerical Methods

A. Continuum Method

A continuum model was used to describe the gas flow in the axisymmetric and three-dimensional nozzles. Numerical solution of the Navier–Stokes equations for viscous fluid flow was obtained with a finite volume spatial discretization on a structured three-dimensional grid implemented in GASP.[10]

Molecular nitrogen is treated as a perfect gas, and the temperature-dependent gas viscosity is obtained from the Sutherland model (see Ref. 11). Viscous derivative terms in the momentum and energy conservation equations are computed with second-order accuracy on the interior and gas–solid interface cells. The third-order, upwind-biased scheme is applied for spatial reconstruction of volume properties on the cell boundaries. To obtain a steady-state solution, two-factor approximate factorization is used for time stepping.[10]

As was shown by Ivanov et al.,[6] an extrapolation boundary condition at the exit of a nozzle can significantly decrease the accuracy of the predicted performance at low Reynolds numbers. Therefore, an exterior region of the nozzle was also included in the present computational domain. Two-zone grids resolving gradients near wall boundaries and along the axis are used in the computations. Grid convergence studies showed that the solution is grid independent for grid dimensions of at least 200×40 (zone 1) and 100×60 (zone 2) for the axisymmetric and two-dimensional cases and $200 \times 40 \times 20$ (zone 1) and $100 \times 60 \times 20$ (zone 2) for the three-dimensional case.

The GASP message passing interface (MPI) capabilities allow iterations in different regions of the computational domain to be performed in parallel. When this option is used on a two-processor SGI Octane, the total computational time for the axisymmetric case with the aforementioned axisymmetric grid is ~8 h and ~50 h for the three-dimensional case.

A no-slip boundary condition is used in these computations to model gas–surface interaction at a fixed wall temperature. The temperature of the wall is set to the stagnation temperature at the chamber. The inlet conditions are obtained from ideal nozzle theory based on stagnation gas properties and an inlet area ratio. For the axisymmetric case, both subsonic and critical inlet conditions are considered. It was found that for the subsonic inlet conditions the boundary layer is thin compared to the the nozzle throat dimension. Hence, the difference between the flowfield solutions for these two types of inlet conditions is expected to be small. Figure 3 shows a comparison of the Mach number fields for the subsonic and critical inlet conditions except for regions close to the throat; the spatial distribution of Mach numbers is similar for both cases. Table 2 shows that the nozzle performance characteristics of the axisymmetric nozzle for both conditions are also similar.

The constant critical throat condition is, therefore, used as the boundary conditions for the axisymmetric and three-dimensional solutions calculated with the Navier–Stokes and DSMC methods.

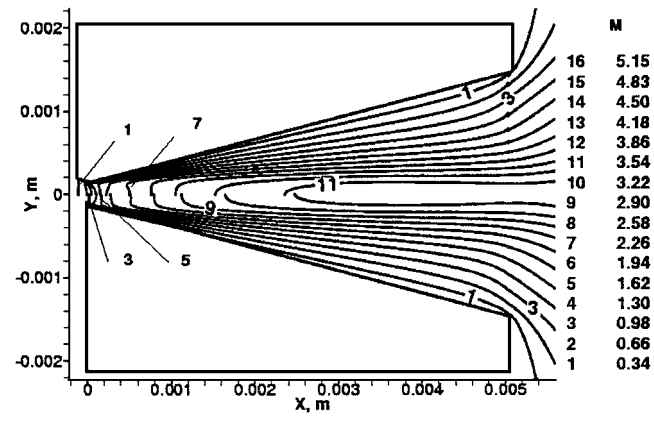

Fig. 3 Mach number fields for uniform and nonuniform throat conditions.

Table 2 Axisymmetric nozzle performance characteristics for continuum solutions

Location	Thrust, mN	I_{sp}, s
Subsonic inlet	1.08	66.06
Uniform throat	1.07	65.62

B. DSMC Method

The DSMC method[12] is a statistical computational approach used for solving rarefied gasdynamics problems. During the past several years, it has also been successfully applied to modeling flows in the near-continuum regime. In this work, a DSMC-based software SMILE[13] is used in all DSMC computations. The majorant frequency scheme[14] of the DSMC method is used to model collisions between molecules. A variable soft sphere is assumed to be the intermolecular potential model.[15] The Larsen–Borgnakke model[16] with temperature-dependent rotational and vibrational collision numbers and discrete rotational and vibrational energies is used for the energy exchange between translational and internal modes.

Under the flow and geometry conditions examined in this work, gas–surface interactions are expected to affect the flow significantly. The DSMC technique allows a detailed treatment of this interaction. Gas molecules can lose or gain a fraction of impulse and energy on a collision with a surface, and the outcome of the collision depends on physical and thermal properties of the surface and gas. An ideally smooth surface would reflect particles specularly with the reflection angle equal to the incident angle, and the magnitude of the momentum components remain the same. Real surfaces have a significant degree of roughness at the molecular scale that results in inelastic diffusive collisions of a molecule with the surface.

One of the most widely used gas–surface interaction models, the Maxwell model, assumes that a fraction $(1 - \alpha_d)$ of incident particles is reflected specularly while the remaining fraction α_d experiences diffuse reflection, that is, particle velocities are distributed according to the Maxwellian distribution with the surface temperature. This parameter α_d is equal to the tangential momentum accommodation coefficient:

$$\alpha_d = (P_{i\tau} - P_{r\tau})/P_{i\tau}$$

where P_τ is the tangential momentum and indices i and r refer to incident and reflected particles. Experimental data[17] for silicon interacting with a nitrogen flow suggest an accommodation coefficient of $\alpha_d = 0.8$. The Maxwell model with different values of α_d between 0 and 1 and the surface temperature $T_w = 300$ K is used in the DSMC computations.

The degree of energy (or thermal) accommodation of the gas with the surface can also be modeled in a similar manner. The thermal accommodation factor α_E was assumed to be unity for the diffuse tangential momentum model.

The majorant frequency scheme used in SMILE was strictly derived from the Leontovich master kinetic equation for the N-particle distribution function. In any system of a finite number of particles, N, there are statistical correlations between particles[18] that arise even when particles were initially independent. The master kinetic equation differs from the Boltzmann equation, the principal equation that describes rarefied gas flows, by the presence of a source term dependent on a pair correlation function, $g = f_2 - f_1 f_1$. Here, f_1 and f_2 are one- and two-particle distribution functions, respectively. The correlation function $g \propto N^{-1}$, and therefore, the correlation term vanishes when $N \to \infty$.

The statistical dependence is inherent in any system of N particles. The number of simulated particles is, therefore, a crucial parameter for any DSMC study. There should be enough particles in the simulation so that the statistical correlations do not affect the result of the simulation and so that it can be considered a solution of the Boltzmann equation. It was suggested by Gimelshein et al.[19] to use the number of molecules in a cube with the linear dimension of the local mean free path λ as an estimate for statistical correlations. Usually, there should be a few molecules in λ^3 for the correlations to be negligible. Therefore, the number of particles required is especially severe when the DSMC method is applied to model three-dimensional near-continuum flows. These requirements are connected with both the flow dimensionality and high density of the gas, that is, small λ.

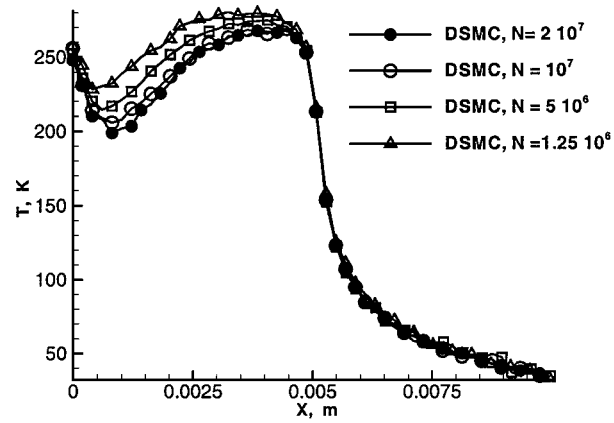

Fig. 4 DSMC translational temperature profiles in the three-dimensional micronozzle for different numbers of particles.

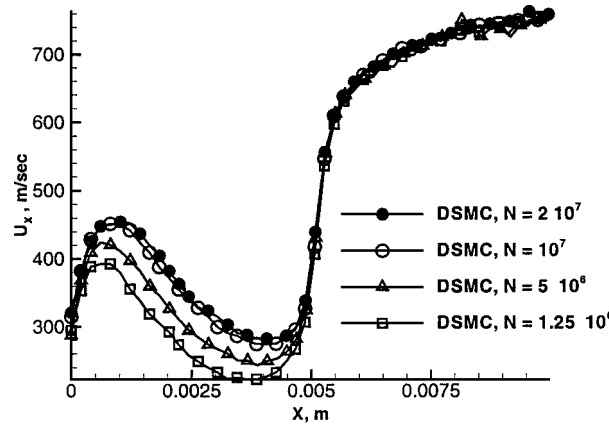

Fig. 5 DSMC velocity component U_x profiles in the three-dimensional micronozzle as a function of the number of particles.

Thus, it is important to analyze the influence of the number of particles to have results independent of particle correlations. Convergence studies of the DSMC solution in terms of the number of particles were conducted for the three-dimensional micronozzle. The translational temperature and the X-velocity component U_x profiles along the nozzle centerline are plotted in Figs. 4 and 5 for different numbers of simulated particles in the computational domain: $N = 1.3 \times 10^6, 5 \times 10^6, 1 \times 10^7$, and 2×10^7. The simulations show that there is a dependence of the translational temperature and velocity on N in the region of high flow density. It is seen from the profiles that the DSMC solution for a smaller number of particles is shifted. However, the results show that the solutions are essentially the same for $N = 10^7$ and 2×10^7 particles and that convergence has been obtained.

In general, the DSMC calculations presented here were carried out with the following numerical parameters. Both adaptive rectangular grids were used for collisions and macroparameters sampling with a total of approximately 10^6 collisional cells used. A time step of 0.5×10^{-9} was used, and the total number of the sampling time steps was 80,000.

IV. Results and Discussion

A. Axisymmetric Conical Nozzle

Let us consider the flow in an axisymmetric conical micronozzle that was studied with the continuum and DSMC methods. A comparison of density fields obtained by the two techniques is given in Fig. 6. The density is normalized by its value at the nozzle throat.

The flowfields obtained for the axisymmetric micronozzle are typical for cold-gas thrusters. The gas experiences about two orders

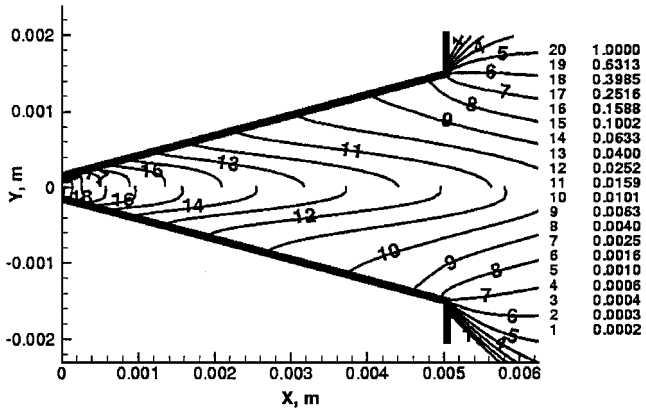

Fig. 6 Normalized number density contours in an axisymmetric micronozzle: DSMC (top) and continuum (bottom).

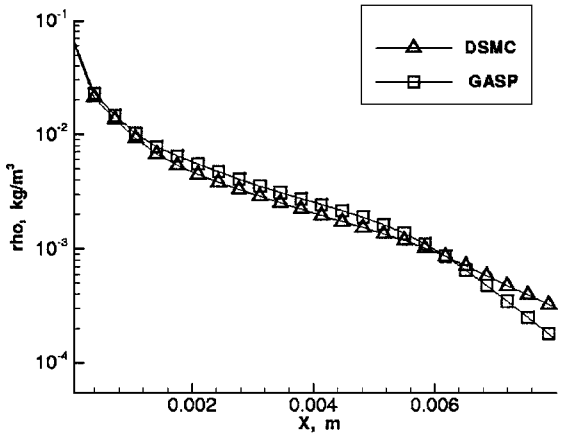

Fig. 7 Comparison of the density profiles along the nozzle axis for the axisymmetric case.

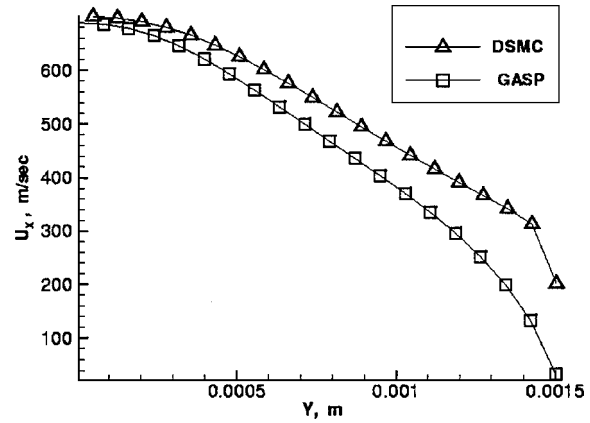

Fig. 8 *X* component of velocity at the nozzle exit plane in the axisymmetric case.

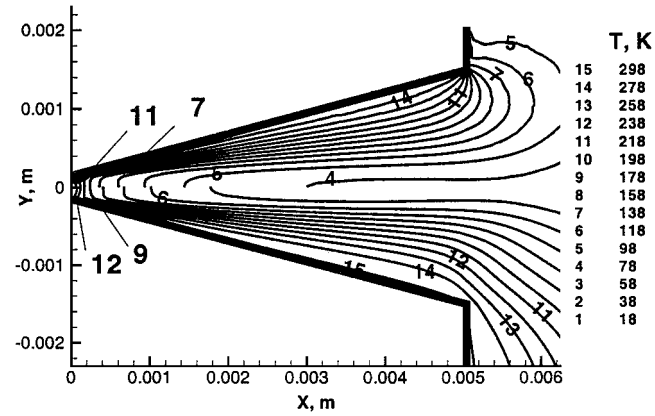

Fig. 9 Translational temperature contours (Kelvin) in the axisymmetric micronozzle computed with DSMC (top) and continuum (bottom) flow models.

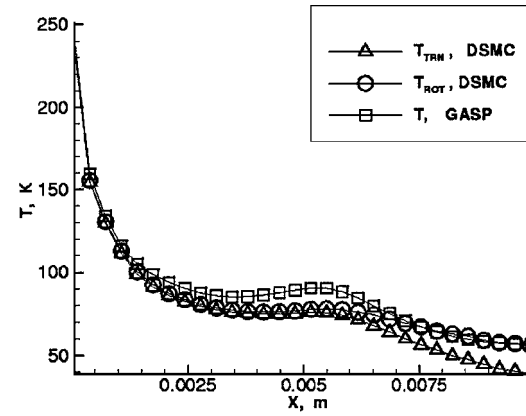

Fig. 10 Comparison of temperature profiles along the nozzle axis for the axisymmetric case.

of magnitude decrease in density along the nozzle axis (see Fig. 7). In the radial direction, the density decreases near the wall because the temperature of the wall is higher than that of gas. Axial velocity fields for the DSMC and Navier–Stokes solutions were studied. It was observed that the numerical solution of Navier–Stokes equations agrees well with the DSMC results inside the nozzle and in the core flow outside the nozzle. There is a significant difference between the two solutions only in the region of the nozzle lip due to the rapid expansion of the gas and a high flow rarefaction that is difficult to capture by continuum methods.

Velocity contours qualitatively illustrate the growth of the boundary-layer thickness downstream from the nozzle throat. To study the boundary-layer growth in more detail, the distribution of the X component of velocity at the nozzle exit is given in Fig. 8. The velocity gradient is large close to the axis, and the boundary layer occupies most of the exit area. The difference between the velocities at the wall for the two approaches is due to the difference in their boundary conditions. However, comparison of the velocity profiles along the nozzle axis shows a small difference between the two solutions.

Translational temperature contours are shown in Fig. 9 for the two different flow models. The agreement is satisfactory inside the nozzle except in the vicinity of the lip, where the impact of flow rarefaction is again significant. The GASP solver assumes there is an equilibrium between translational and rotational modes. The vibrational mode is essentially frozen at the low temperatures under consideration, and vibrational excitation is not an important factor; however, the rotational temperature may be significantly different from the translational one. Figure 10 shows the DSMC rotational and translational temperature profiles along the nozzle axis compared with the translational temperature profile obtained by GASP. Differences between the translational and rotational temperatures beyond the nozzle exit can be observed. The difference between the translational temperatures obtained by the continuum and kinetic approaches is due to rarefaction and wall effects.

B. Flow in a Flat Micronozzle Computed Using Two- and Three-Dimensional Models

A two-dimensional model can be used to describe the flow in a nozzle of a flat geometric configuration if the influence of the end walls [the nozzle surfaces located in the x–y planes at $z = 0$ and h (Fig. 1)] is negligible. However, as was shown in the preceding section for an axisymmetric flow, the entire area of the nozzle exit is affected by the wall boundary layer. In the flat nozzle case with the same flow conditions at the throat, an even larger impact of viscous effects can be anticipated because of a greater surface area to volume ratio. Full three-dimensional flow modeling is, therefore, required

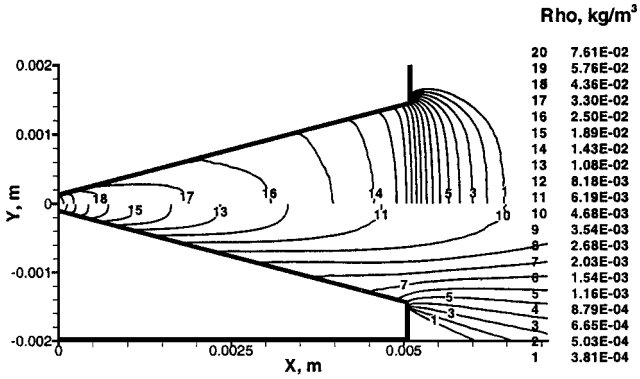

Fig. 11 Density contours in a flat micronozzle computed for three-dimensional (top) and two-dimensional (bottom) cases by the DSMC method.

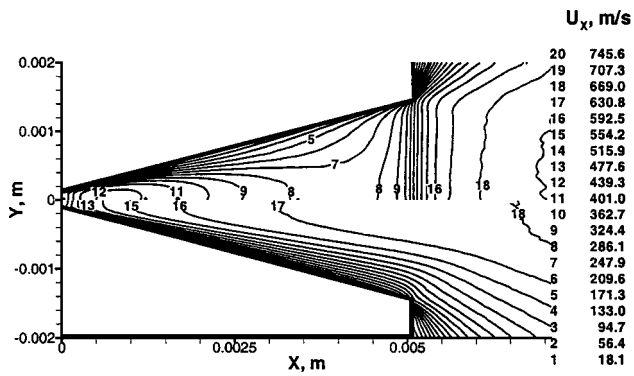

Fig. 12 Contours of velocity component in the X direction for a flat micronozzle calculated using the three-dimensional (top) and two-dimensional (bottom) models.

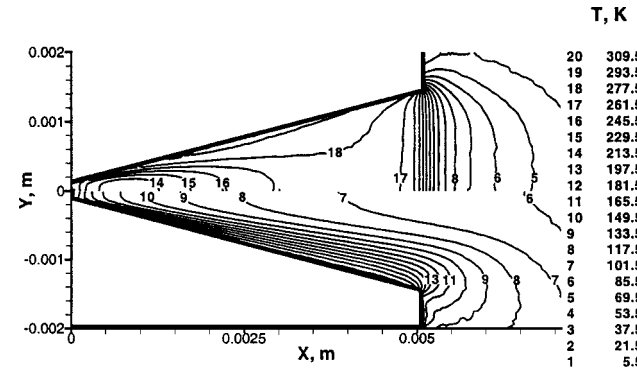

Fig. 13 Translational temperature contours for a flat micronozzle calculated using the three-dimensional (top) and two-dimensional (bottom) flow models.

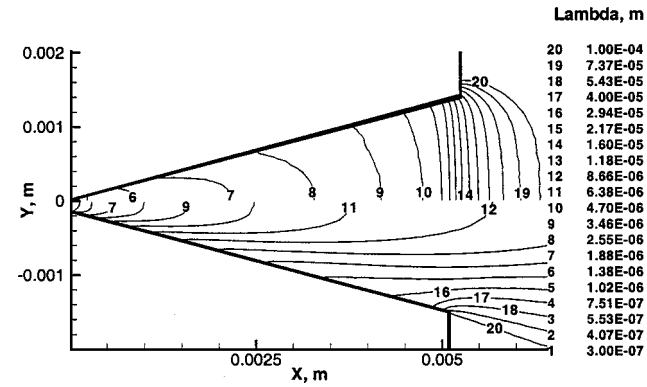

Fig. 14 Mean free path contours for a flat micronozzle calculated using the three-dimensional (top) and two-dimensional (bottom) flow models.

to simulate the gas flow and to predict accurately the performance characteristics of a three-dimensional high aspect ratio micronozzle.

To examine the contribution of the third dimension at the given conditions, the modeling of two-dimensional and three-dimensional flows in a flat micronozzle was conducted using the continuum and kinetic approaches. The computational grid for the two-dimensional flow is the diverging nozzle portion of Fig. 2. The density contours are shown in Fig. 11 for both the two- and three-dimensional flow models. Whereas the density decreases gradually in the two-dimensional case, the flow in the three-dimensional nozzle experiences two successive expansions, at the nozzle throat and the exit. This is due to the contribution of two different processes, viscous dissipation and flow expansion. Pressure fields for the two- and three-dimensional flow models were also found to be significantly different. The pressure is higher inside the nozzle for the three-dimensional case due to wall effects, and the core flow values are approximately seven times larger. In the expansion region, downstream of the nozzle exit, the pressure is lower for the three-dimensional case because the flow expands in three dimensions.

A comparison of velocity fields for the two cases is given in Fig. 12. As expected, the two-dimensional model predicts the values of the velocity component in X direction to be larger inside the nozzle. For the three-dimensional case, the velocity first increases at 1 mm downstream from the throat (the flow expansion dominates there) and then slightly decreases toward the exit because the wall effects become more important. The velocity has a local maximum of 450 m/s at ~1 mm from the throat. The flow expands rapidly after the exit, and the velocity at 2 mm from the exit is even greater than the corresponding velocities in the two-dimensional case.

Figure 13 shows that the translational temperature fields are also qualitatively different for the two flow cases. The temperature decreases downstream in the direction of the nozzle axis and increases at the wall (the gas is cooler than the surface) for the two-dimensional case. There is a local minimum of temperature at 1 mm from the throat in the three-dimensional flow, and temperature values are generally higher inside the nozzle and lower downstream from the exit plane for this case. The influence of the end walls is, therefore, very important for the height to width ratio considered. For larger ratios, a smaller effect would be expected, and likewise there should be a smaller difference between the temperature fields predicted by the two- and three-dimensional models because the difference in the expansion process would also be reduced.

The difference in the expansion process is shown in Fig. 14, where the molecular local mean free path is plotted. The mean free path increases gradually inside the three-dimensional nozzle. It changes by a factor of three from the throat to the exit. For the two-dimensional case it grows more rapidly in the X direction, and there is also a strong growth across the nozzle near the walls. Note that the local characteristic length for the three-dimensional case is equal to the nozzle height $h = 300$ μm. The local Knudsen number at the exit plane is, therefore, about 0.1, which falls into a regime where the continuum model fails.

C. Wall Effects in Axisymmetric and Three-Dimensional Nozzles

To choose reasonable geometric parameters that will create a flow that expands through a micronozzle with minimal surface losses, an estimate of the boundary-layer thickness at the exit has to be made. A possible approach to nozzle design could be to utilize the flow over a plate for an assessment of the boundary-layer thickness growth. In a nozzle, though, the boundary-layer thickness grows much more rapidly than that over a plate due to the gas expansion. A full simulation is, therefore, required to examine the boundary-layer growth for a specified nozzle geometry and to choose a nozzle configuration that decreases the boundary-layer thickness.

To understand how the boundary layer grows in a three-dimensional nozzle under the chosen conditions, Fig. 15 shows the translational temperature contours at different cross sections perpendicular to the nozzle axis. The viscous layer is developed very rapidly, and at a distance of several throat widths, it occupies the entire cross-sectional area. There is, therefore, no inviscid core in

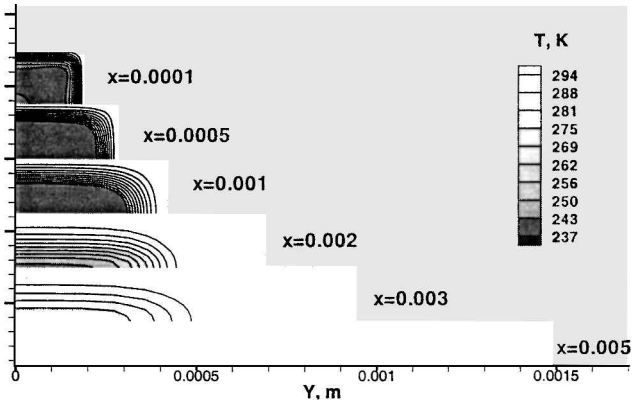

Fig. 15 Viscous layer growth in a flat micronozzle obtained by a three-dimensional DSMC calculation.

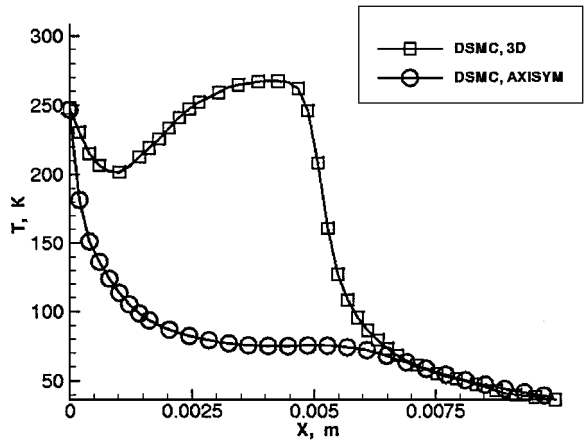

Fig. 16 Translational temperature profile along the nozzle axis for the axisymmetric and three-dimensional nozzles.

the gas flow inside the nozzle at the Reynolds number and aspect ratio modeled in this work.

The wall effects and flow expansion strongly impact the flow in a three-dimensional nozzle as compared to that in an axisymmetric nozzle. Figure 16 shows the translational temperature profiles along the nozzle axis for the three-dimensional and axisymmetric cases. After an initial decrease at the first 1 mm due to the gas expansion, the temperature increases in the three-dimensional nozzle. Such an increase is caused by the viscous dissipation of the flow kinetic energy due to the shear on the walls. Beyond the nozzle exit, where the gas experiences a free expansion into a vacuum, the velocities and temperatures coincide for the two cases because the mass flow rates are equal.

The large difference between the two solutions shown for the temperature profiles is also observed for the velocity fields. The profiles of the velocity in the X direction are presented in Fig. 17. The velocity increases monotonously downstream from the nozzle exit in the two-dimensional case, whereas in the three-dimensional flow, there is a velocity minimum located at $X = 0.004$ m. The increase of temperature (Fig. 16) and decrease in velocity in the three-dimensional nozzle is a consequence of the shear on the walls. For a hypersonic nozzle flow expanding into vacuum, one would expect the extremum to be at the exit plane. However, the extremum is located upstream of the nozzle exit because of the subsonic region at the walls.

These results show that the presence of the walls is very pronounced in the three-dimensional case. The model used to simulate the gas–surface interaction is, therefore, important. Because all results presented earlier were obtained using the tangential momentum accommodation coefficient $\alpha_d = 1$, different values of α_d were also used to examine the possible influence of the surface model. The DSMC computations were performed both for the axisymmetric and three-dimensional nozzles for different values of α_d. A related investigation was performed by Ketsdever et al. for two-dimensional microresistojets.[20]

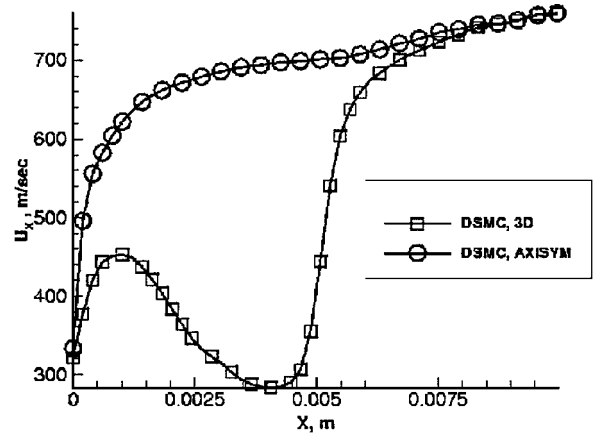

Fig. 17 X-component velocity profile along the nozzle axis for the axisymmetric and three-dimensional nozzles.

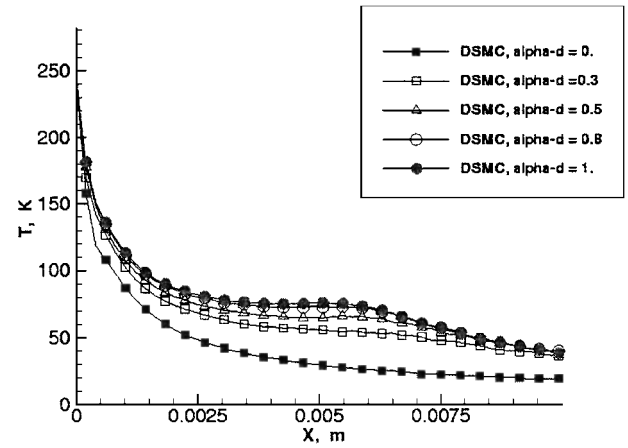

Fig. 18 Translational temperature profiles along the nozzle axis for different α_d in an axisymmetric micronozzle.

Translational temperature profiles along the nozzle axis for different α_d are shown in Fig. 18. The temperature increases with α_d. There is a qualitative difference between the solution for $\alpha_d = 0$ (ideally smooth surface) and any nonzero α_d for which the profile has a kink after the nozzle exit. There is also a visible difference between $\alpha_d = 0$, 0.3, and 0.5 profiles. Experimental work by Arkilis[17] suggests that a value of $\alpha_d = 0.8$ is suitable for a nitrogen flow in a silicon microchannel. The result for an axisymmetric nozzle flow with $\alpha_d = 0.8$ is very close to the solution with $\alpha_d = 1$.

The flow solution for the three-dimensional case can be expected to show a greater dependency on the gas–surface interaction model because wall effects dominate the flow inside the nozzle. The DSMC temperature and density flowfields for $\alpha_d = 0.8$ and 1 values were studied. There is a subtle difference in the core flow, but generally the temperatures and densities are very close for these two cases. The specific impulse for these two cases was calculated, and the difference was found to be less than 1%.

D. Micronozzle Performance and Comparison with Experiment

The calculated thrust levels and specific impulses for different micronozzle simulations are summarized in Table 3. For the cases considered, the GASP solution slightly overpredicts the thrust values obtained by the DSMC method (by several percent). When axisymmetric and three-dimensional results are compared, the thrust, as well as the specific impulse, are lower for the flat micronozzle. The wall effects in the three-dimensional case also cause an approximate 20% reduction in thrust as compared to the two-dimensional model. Note that the two-dimensional model gives the highest thrust values for the three cases under consideration. The specific impulse is also

Table 3 Comparison of nozzle performance characteristics for different flow models

Case	Thrust, mN	I_{sp}, s
AS GASP	1.07	65.62
AS SMILE	1.03	65.50
Two-dimensional GASP	1.17	69.45
Two-dimensional SMILE	1.10	68.74
Three-dimensional SMILE	0.93	56.61

Table 4 Summary of experimental data of Reed et al.[8]

Area ratio	Reynolds number	Throat dimension, width × depth, μm	Thrust, mN
1.0	183	372 × 295	0.9045
1.5	199	230 × 271	1.125
4.8	272	367 × 198	1.150
9.7	207	362 × 260	1.105

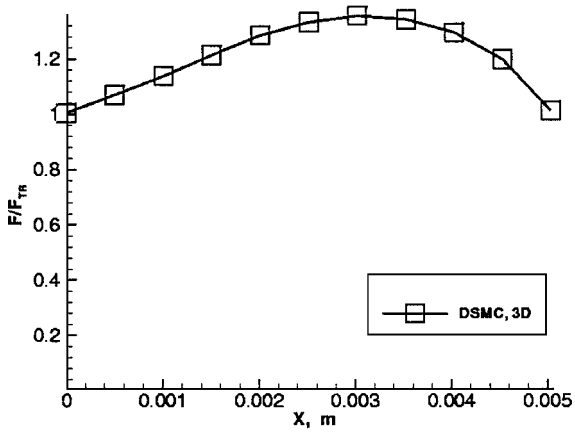

Fig. 19 Total impulse flux at different axial locations inside a three-dimensional micronozzle normalized by the throat value.

highest for the two-dimensional model (5% greater than for the axisymmetric nozzle and 20% greater than for the three-dimensional nozzle).

The total impulse flux at different locations downstream of the throat of the three-dimensional nozzle obtained by the DSMC method is plotted in Fig. 19. There is an undesirable reduction in thrust in the second half of the nozzle caused by the viscous losses. The way to increase the performance would be to make the micronozzle shorter or to increase its height.

Finally, the calculated thrust for the three-dimensional micronozzle is now compared with recently available experimental data close to Reynolds number of 2×10^2. The measurements of thrust for silicon fabricated nozzles were conducted at NASA John H. Glenn Research Center at Lewis Field.[8] The intended geometric design of the micronozzles was the same as described in Fig. 1 with the throat dimension of 300 × 300 μm. The actual size of the fabricated thrusters varied due to the difficulties of miniature silicon etching. Before the testing, the throat dimensions were measured using a measuring microscope technique. A number of thrusters were then tested with gaseous nitrogen at room temperature in a vacuum facility. Further details may be found in Ref. 8. Table 4 summarizes the specific experimental conditions of the data used in the comparison with the three-dimensional nozzle calculation presented here. Note that the modeling was conducted for a Reynolds number of 2×10^2 at the throat. Thrust measurement accuracy was on the order of 3%.

Figure 20 shows the comparison of calculated thrust at different axial stations and measured thrust for the corresponding area ratio nozzles. The computational results are in good agreement with the experimental thrust measurements. The calculated thrust is a maximum at approximately 60% of the nozzle length, which corresponds to an area ratio of 6. Additional comparisons between data and modeling are necessary, but the comparison shown in Fig. 20 suggests that there is an agreement in the thrust axial dependence.

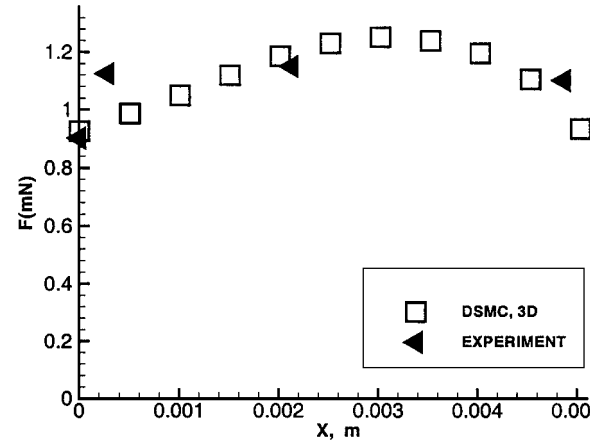

Fig. 20 Comparison of measured and calculated total impulse flux at different axial locations inside a three-dimensional micronozzle.

V. Conclusions

A numerical study of two different geometric configurations of micronozzles, axisymmetric and three dimensional, has been conducted for a throat Reynolds number of 2×10^2 using the kinetic (DSMC method) and the continuum (solution of Navier–Stokes equations) approaches. A convergence study was performed for the DSMC method to reduce the statistical dependence between particles and to obtain a solution independent of the number of simulated particles. The significance of statistical dependence becomes critical in the three-dimensional case, where it was found that it is necessary to use at least 20×10^6 particles to have a particle-independent solution.

The DSMC and Navier–Stokes solutions are in a satisfactory agreement for the two-dimensional flow inside the nozzle. There is a significant difference between them in the region near the lip where the flow expands rapidly. The use of an external zone in the continuum approach, which starts at the nozzle exit and expands downstream, allows one to eliminate the possible impact of the extrapolation outflow boundary condition at the nozzle exit. This results in thrust values that are in agreement with those obtained by the DSMC method.

Both the subsonic inflow conditions and critical throat conditions were considered in the continuum computations. The calculated flowfields and nozzle performance were shown to be insensitive to the type of inflow conditions.

The effect of the gas–surface tangential momentum accommodation coefficient on the flow was investigated by the DSMC method. The flow was found to be weakly dependent on this coefficient when it is changed from 0.8 to 1 for both the axisymmetric and three-dimensional cases. The axisymmetric flow changes significantly for accommodation coefficients smaller than 0.5; however, this value of the accommodation coefficient is smaller than the experimental values for a nitrogen flow in a silicon microchannel.

The impact of wall effects on thrust level was examined for axisymmetric and two- and three-dimensional micronozzles. The flow in a flat nozzle has a three-dimensional structure and is strongly influenced by the end walls. The additional gas–surface interaction causes a significant reduction in thrust (about 20%) as compared to the two-dimensional model and an axisymmetric nozzle. Attempts to predict the performance characteristics of a three-dimensional microthruster using a two-dimensional model may, therefore, result in significant design errors.

Comparison of the three-dimensional calculations presented in this work with recent experimental thrust data obtained at Reynolds numbers close to 2×10^2 show good agreement.

Acknowledgments

The work at the Pennsylvania State University and George Washington University was supported by Army Research Office

Grant DAAG55-98-1-009, Space and Naval Warfare Systems Center (SPAWARSYSCEN) San Diego Grant N66001-98-1-8909, and the Ballistic Missile Defense Organization. We would like to thank Clifton Phillips of SPAWARSYSCEN, who provided us with computer time on a Hewlett–Packard V2500 computer. The authors are thankful to M. S. Ivanov for a valuable discussion and his attention to this work.

References

[1]Ho, C., and Tai, Y., "Review: MEMS and Its Applications for Flow Control," *Journal of Fluids Engineering*, Vol. 118, Sept. 1996, pp. 437–447.

[2]Gad-el-Hak, M., "The Fluid Mechanics of Microdevices—The Freemen Scholar Lecture," *Journal of Fluids Engineering*, Vol. 121, March 1999, pp. 5–33.

[3]Bayt, R. L., Breuer, K. S., Lin, L., Forster, F. K., Aluru, N. R., and Zhang, X., "Viscous Effects in Supersonic MEMS-Fabricated Nozzles," *Proceedings of Micro-Electro-Mechanical Systems (MEMS)—1998. ASME International Mechanical Engineering Congress and Exposition*, American Society of Mechanical Engineers, New York, 1998, pp. 117–123.

[4]Boyd, I. D., "Monte Carlo Simulation of Nonequilibrium Flow in a Low-Power Hydrogen Arcjet," *Physics of Fluids*, Vol. 9, No. 10, 1997, pp. 3086–3095.

[5]Chung, C.-H., Kim, S. C., Stubbs, R. M., and De Witt, K. J., "Low-Density Nozzle Flow by the Direct Simulation Monte Carlo and Continuum Methods," *Journal of Propulsion and Power*, Vol. 11, No. 1, 1995, pp. 64–70.

[6]Ivanov, M. S., Markelov, G. N., Wadsworth, D. C., and Ketsdever, A. D., "Numerical Study of Cold Gas Micronozzle Flows," AIAA Paper 99-0166, Jan. 1999.

[7]Ivanov, M. S., and Markelov, G. N., "Numerical Study of Thruster Nozzle Plume," AIAA Paper 2000-0468, Jan. 2000.

[8]de Groot, W. A., Reed, B. D., and Brenizer, M., "Preliminary Results of Solid Gas Generator Micropropulsion," NASA TM–1999-208842.

[9]Reed, B. D., de Groot, W., and Dang, L., "Experimental Evaluation of Cold Flow Micronozzles," AIAA Paper 2001-3521, July 2001.

[10]"General Aerodynamic Simulation Program, Computational Flow Analysis Software for the Scientist and Engineer," GASP Ver. 3, User's Manual, Aerosoft Co., Blacksburg, VA, May 1996.

[11]White, F. M., *Viscous Fluid Flow*, McGraw–Hill, New York, 1974, p. 27.

[12]Bird, G. A., *Molecular Gas Dynamics and Direct Simulation of Rarefied Gas Flows*, Oxford Science, Oxford, 1994.

[13]Ivanov, M. S., Markelov, G. N., and Gimelshein, S. F., "Statistical Simulation of Reactive Rarefied Flows: Numerical Approach and Applications," AIAA Paper 98-2669, June 1998.

[14]Ivanov, M. S., and Rogasinsky, S. V., "Analysis of Numerical Techniques of the Direct Simulation Monte Carlo Method in the Rarefied Gas Dynamics," *Sov. J. Numer. Anal. Math. Modeling* Vol. 2, No. 6, 1988, pp. 453–465.

[15]Koura, K., and Matsumoto, H., "Variable Soft Sphere Molecular Model for Inverse-Power-Law of Lennard–Jones Potential," *Physics of Fluids A*, Vol. 3, No. 10, 1991, pp. 2459–2465.

[16]Borgnakke, C., and Larsen, P. S., "Statistical Collision Model for Monte Carlo Simulation of Polyatomic Gas Mixture," *Journal of Computational Physics*, Vol. 18, 1975, pp. 405–420.

[17]Arkilis, E. B., "Measurement of Mass Flow and Tangential Momentum Accommodation Coefficient in Silicon Micromachined Channels," Ph.D. Dissertation, Dept. of Aeronautics and Astronautics, Massachusetts Inst. of Technology, Cambridge, MA, Jan. 1997.

[18]Ivanov, M. S., Rogasinsky, S. V., and Rudyak, V. Y., "Direct Statistical Simulation Method and Master Kinetic Equation," *Proceedings of the 16th International Symposium on Rarefied Gas Dynamics*, edited by E. P. Muntz, D. P. Weaver, and D. H. Campbell, AIAA, Washington, DC, 1989, pp. 171–181.

[19]Gimelshein, S. F., Ivanov, M. S., and Rogasinsky, S. V., "Investigation of Shock Wave Structure by Majorant Cell and Free Cell Schemes of DSMC," *Proceedings of the 17th International Symposium on Rarefied Gas Dynamics*, VCH, Weinheim, Germany, 1991, pp. 718–726.

[20]Ketsdever, A. D., Wadswoth, D., and Muntz, E. P., "Influence of Gas–Surface Interaction Models on Predicted Performance Characteristics of a Micro-Resistojet," AIAA Paper 2000-2430, June 2000.

M. Sichel
Associate Editor